PHYSOR 2018: Reactor Physics paving the way towards more efficient systems
Cancun, Mexico, April 22-26, 2018

NEW SODIUM FAST REACTOR NEUTRONICS BENCHMARK

A. Ponomarev, A. Bednarova,[*] K. Mikityuk

Paul Scherrer Institute
CH-5232 Villigen

alexander.ponomarev@psi.ch

ABSTRACT

Fast reactor technology aimed on improved safety and sustainability as in accord to the goals of Generation IV candidates [1], places specific requirements on the validating the codes which are used for evaluation of the performance and behaviour of such systems. A new calculation benchmark has been proposed for the startup core of the Superphénix reactor. The paper gives an overview of the benchmark content, provides the core model definition for static neutronics calculations and presents preliminary results on core performance and comparisons with some experimental data, obtained during startup trials. The calculation results allowed concluding that the developed model can serve as an appropriate basis for benchmark activity.

KEYWORDS: SFR, SPX startup tests

1. INTRODUCTION

The sodium-cooled fast reactor Superphénix (SPX) with its 358 fuel subassemblies (SAs) and about 5.7 tons of plutonium was the largest ever constructed liquid metal cooled reactor in the history of nuclear energy production (see Fig. 1). The construction works started in 1977 in the area of Creys-Malville near Lyon in France within the reach of the river Rhone. After about eight years of build-up and preparation, the first critical state was achieved. In 1986 the power plant started to generate electricity and on December 9, 1986 reactor reached the full power level. During its operation time, countless experiments and measurements were conducted and considerable amount of precious data from the lifetime of large fast reactor were collected. This data should not be forgotten but employed in order to validate the codes calculating the fast reactors.

The first set of the measurements were gained during the start-up tests organized in four phases [2] as a transition between the construction progressive completion and reaching the rated power. The last fourth phase has included an extensive program with numerous tests carried out during few months of commissioning after the first core SAs have been loaded, so as to measure the core characteristics, the neutron fluxes, the power distributions, the control rod worth and the responses to transients with feedback coefficient determination.

In frame of the Horizon-2020 ESFR-SMART EU project [3], a new calculation benchmark of the SPX core is proposed for validation of calculation tools. The results of the benchmark are expected to

[*] Current affiliation: State Office for Nuclear Safety, Prague, Czech Republic

contribute to and allow better understanding of the neutronics and thermal hydraulics modelling aspects of a large sodium-cooled fast reactor core at static and transient conditions. An advantage of experimental results was taken in order to prove the accuracy of the model. The benchmark will consist of two main parts, which are static neutronics and transient analysis of the core behaviour.

In this paper, the core specification for static neutronics modelling is presented as a first part of the benchmark which aims to validate calculation tools used for evaluation of neutron physics characteristics of the core: criticality, power spatial distribution, worth of control rods (CRs), reactivity feedback coefficients using available experimental measurements, where possible. Cross-comparisons between different codes results and comparison with experimentally observed core characteristics will provide effective basis for analysis of both quality of the models and calculation tools performance. The core neutron physics characteristics obtained in the first phase will define neutronics basis for the second part devoted to transient analysis [4].

Heterogeneous core model for neutronics is proposed as a reference geometry which is to be adopted in accord to the input of different calculation tools. Thus it may consider additional homogenization procedure for some detailed parts of the geometry. Primary circuit description considers multi-channel core representation with appropriate boundary conditions at core inlet and core outlet. Assumptions needed on modelling of thermal expansion of core elements, fuel properties are to be formulated.

After the introduction, where main Superphénix reactor characteristic and description of available data are given, the second chapter provides details on the core specification developed, including geometry data and materials content, as well as an overview of the assumptions and reference data taken into account for preparation of the core model. Third chapter summarizes some results including comparison with experimentally obtained values. In the last chapter the main findings are summarized and outlook on the next steps of the benchmark is given.

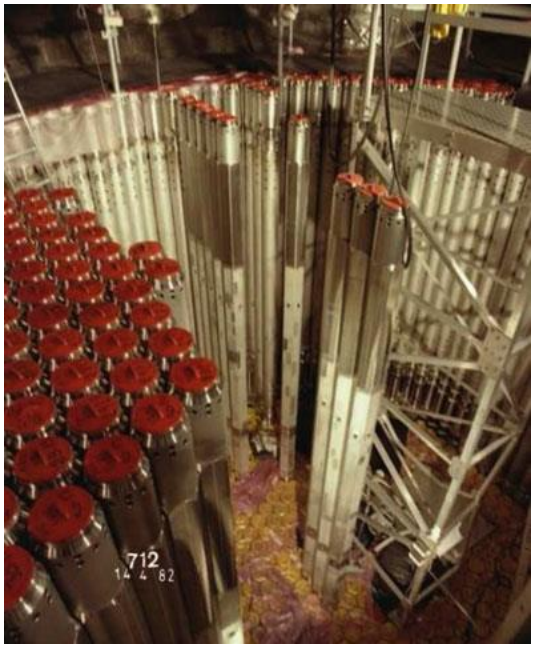

Figure 1. View of the SPX reactor core when being loaded with dummy fuel sub-assemblies but with a part of the core in its final form: the fertile S/A, neutron shielding, etc. [2]

2. SUPERPHÉNIX CORE AND STATIC NEUTRONICS BENCHMARK DESCRIPTION

2.1. General Parameters of the Core

Table I summarizes general parameters of Superphénix reactor core as reported in [5] as well as the nominal operating conditions defined as the basis for the static neutronics benchmark.

Table I. General parameters of the Superphénix reactor core

Parameter	Unit	Value
Thermal / electric power	MW	2990 / 1242
Average fissile / fertile fuel temperature	°C	1227 / 627
Primary sodium inlet / outlet temperature	°C	395 / 545
Fissile/fertile fuel	-	$(U,Pu)O_2$ / UO_2
Intrinsic density of fuel pellet (fissile/fertile)	%TD	95.5
Fissile fuel density	%TD	82.6
Axial blanket fertile fuel density	%TD	87.9
Radial blanket fertile fuel density	%TD	91.6
Stoichiometry ratio O/M	-	1.98
Fissile fuel enrichment in the inner / outer subcore	%	16.0*/19.7*
Total mass of plutonium in the fissile core	kg	5780
Mass of Pu-239 isotope in the fissile core	kg	4054
Mass of U-235 isotope in the fissile core	kg	142
Volume of the fissile core	m^3	10.75
Equivalent diameter of the fissile core	m	3.70
Height of the fissile pellet stack	m	1.00
Height of the lower/upper breeder blanket	m	0.30 / 0.30
Height of the radial blanket fertile pellet stack	m	1.60
Number of subassemblies in the inner/outer subcore	-	193**/171**
Number of subassemblies in the radial breeder blanket	-	234**
Number of control rods (CSD/DSD)	-	21 / 3
Subassembly pitch in the diagrid	mm	179.0

(*) Enrichment is defined as a ration of mass of ^{235}U and all Pu isotopes to mass of all heavy metal isotopes, differs from considered in the benchmark

(**) Differs from considered start-up core configuration

There is a lack of detailed specification of the first core load available in open literature sources. Therefore a number of assumptions based on the engineering judgements had to be made during the benchmark specification development. These assumptions were done using the following check list:

- fuel inventory is consistent with [5];
- initial first core reactivity evaluated at 180°C is as reported in [6];
- reactivity effects of transition from 180C to hot zero power (HZP) and hot full power (HFP) conditions are as reported in [7].

The data of a homogenized core benchmark [8] has also been used as basis for definition of core configuration and material content.

2.2. Definition of the Core Model

2.2.1. Core axial and radial layout specification

The core layout which corresponds to the experimental program at start-up is defined as shown in Fig. 2. In current layout the neutron guide assemblies were neglected as compared to the layout, given in [8] and changed into radial breeder assemblies. Axial structure of the different SAs in the model along with axial

zones dimensions corresponding to as-fabricated geometry is given in Fig. 3. The zones described in the benchmark model as heterogeneous structures are marked with HET, while zones having a homogeneous description are marked with HOM. All HET zones of the model consider detailed SA structure arranged with the given diagrid pitch in plane and sodium outside hexcan. The CSD rods in Fig. 3 are shown at the parking position, which is at the top of the fissile core. Since there is lack of design data for the DSD rods in open literature, the same heterogeneous design was assumed for the DSD rods as for the CSD ones. The length of DSD rod absorber is assumed 1000 mm and all three rods are considered at the upper parking position at the top of the upper axial blanket.

2.2.2. Subassemblies geometry specification

The radial cross sections of the fissile and fertile pin bundles as well as CSD SA are shown in Fig. 4. The axial and radial dimensions are shown in Fig. 3 and Table II, respectively. Using the data of Tables I and II the material volumetric fractions have been calculated in the fuel zones of the core, which are given in Table III for reference. The axial sectioning of the SAs has been established on the basis of data in [5], [9], [10] and [11]. The fissile pin section has a height of 2700 mm and includes the following axial regions (see Fig. 3 and Table II for the dimensions):

- Lower pin plug, modelled as a solid cylinder;
- Lower gas plenum, modelled as an empty pin cladding;
- Fuel pellet support, modelled as a hollow cylinder with inner hole diameter of 5.0 mm
- Solid fertile pellet stack of lower axial blanket with geometry of the pellet and cladding;
- Hollow fissile pellet stack;
- Solid fertile pellet stack of upper axial blanket;
- Upper gas plenum, modelled as an empty pin cladding;
- Upper pin plug, modelled as a solid cylinder.

The equivalent outer diameter of all rods has been used in the calculations to take into account additional steel material of the spacer wire. The lengths of the gas expansion plena as in [11] fit to provide the total fission gas plena volume of 43 cm^3 as in accord to data in [5]. Sodium plenum above the pin section is intended to model the sodium flow transition section from the pin bundle to the outlet section and modelled as an empty hexcan structure. The outlet section represents upper steel shielding of the subassembly. It is modelled as a solid sleeve having outer dimension of the hexcan and inner sodium flow path of 70 mm in diameter.

The modelled pin section of the blanket SA with length of 1900 mm includes the same axial regions as the fissile SA except the hollow fissile pellet stack (Table II and Fig. 5). As in case of the fissile SA, there is no complete data set available on the fertile SA design. The total length of the gas expansion plena has been evaluated to provide the total fission gas plena volume of 40 cm^3 as in accord with [5]. For simplicity, the upper gas plenum, upper pin plug, sodium plenum above the pin section and the outlet section are chosen to be identical to the ones of the fissile SA. The inlet section has the same design as the outlet one.

CSD SA is modelled as a hexcan structure with the absorber rod body inside the hexcan at axial curtain position. The absorber rod body is modelled as an absorber pin bundle within cylindrical sleeve (Table II and Fig. 6). The sleeve dimensions used are found in [2]. There is no data found on the absorber pellet outer diameter and it has been adjusted to ensure an appropriate reactivity worth of the CSD rods as compared to the experimentally observed value of about 8600 pcm [12]. There is no complete data set available on the design of the diluent SAs and radial reflector SAs. The homogenized compositions for these regions as provided in [8] have been taken as basis. The inlet and outlet sections are unified with other SAs and have heterogeneous design, as described above for the fissile and fertile SAs.

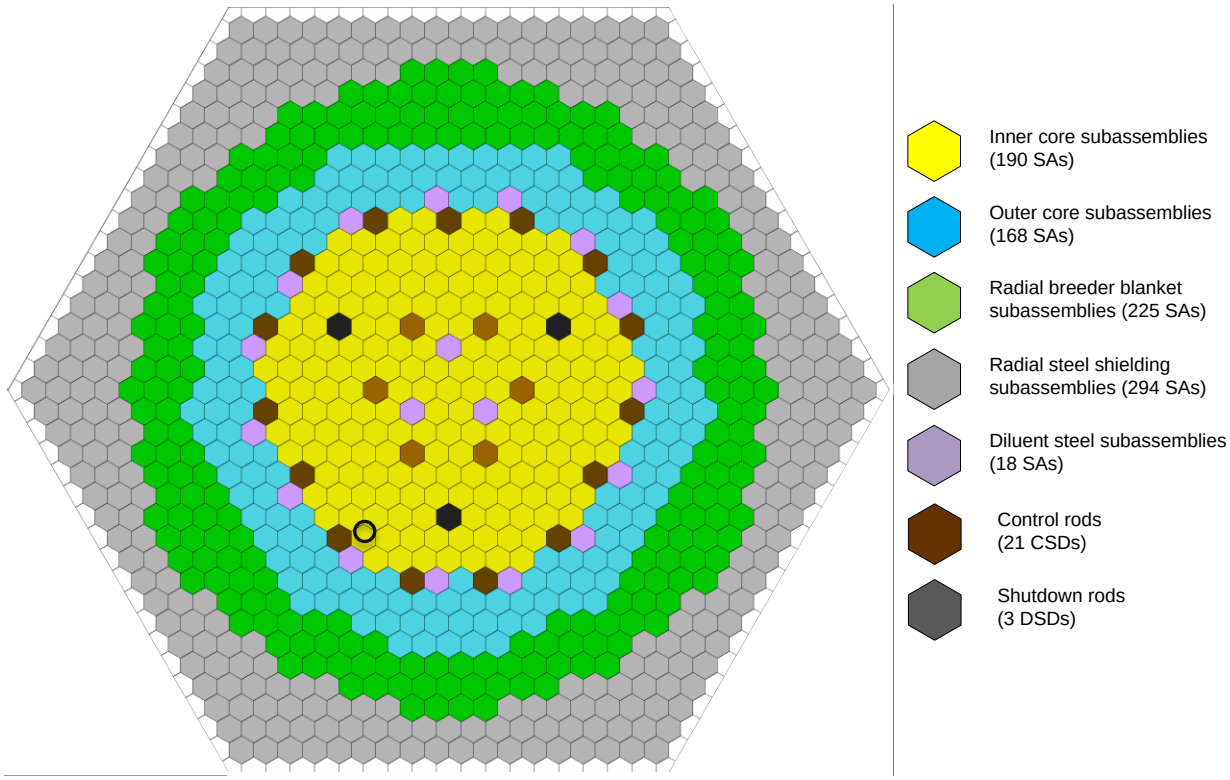

Figure 2. Subassembly arrangement in the model of the start-up core

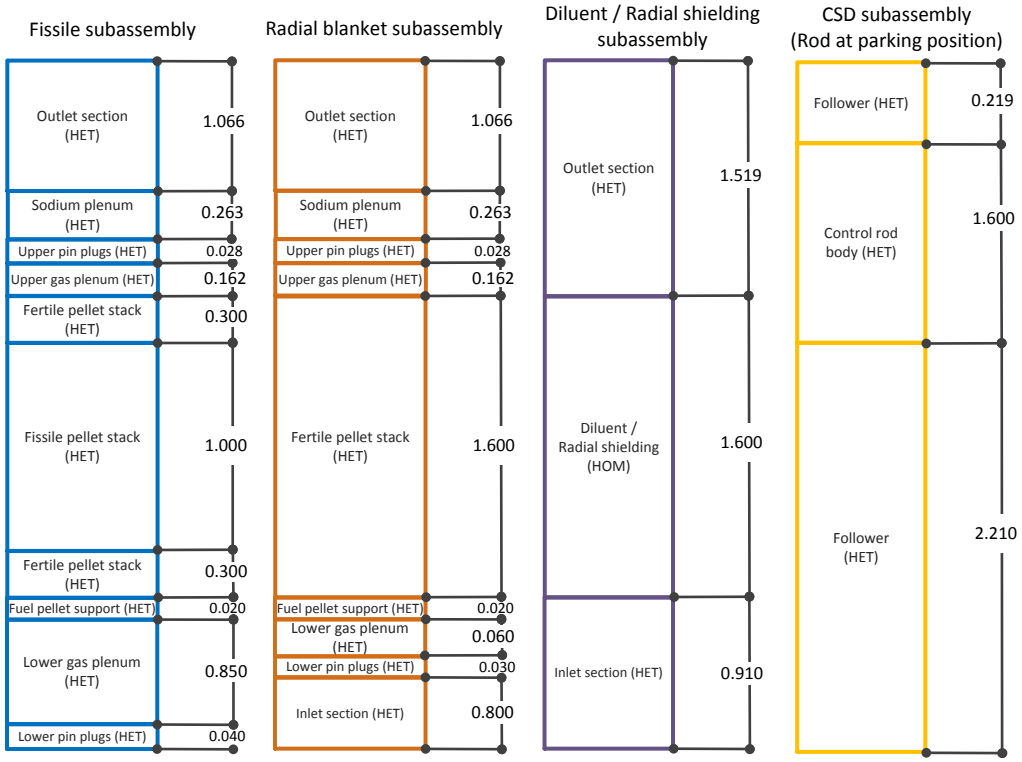

Figure 3. Axial structure of different subassemblies in the model

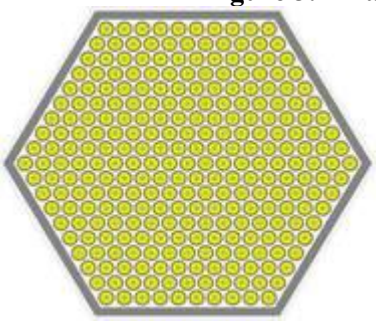

Figure 4. Fissile SA cross section

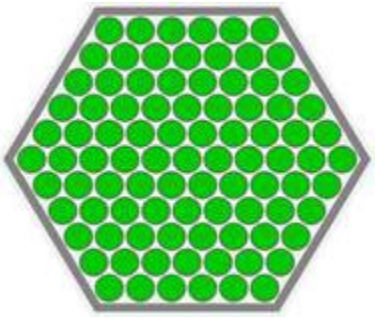

Figure 5. Radial breeder blanket SA cross section

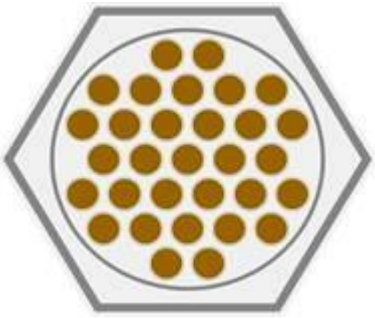

Figure 6. CSD SA cross section

Table II. As-fabricated radial dimensions of fissile, radial breeder blanket and CSD subassemblies

Parameter	Unit	Fissile	Blanket	CSD
Hexcan outer flat-to-flat size	mm	173.0	173.0	173.0
Hexcan wall thickness	mm	4.5	4.5	4.5
Number of pins	-	271	91	31
Pin pitch	mm	9.8	16.9	22.77
Spacer wire diameter	mm	1.2	1.1	-
Pin cladding inner diameter	mm	7.37	14.66	18.0
Pin cladding outer diameter	mm	8.50	15.80	19.0
Pin cladding thickness	mm	0.565	0.57	1.0
Pin cladding outer diameter accounting for spacer wire	mm	8.584	15.838	-
Fissile fuel pellet diameter	mm	7.14	-	-
Fissile fuel pellet inner hole diameter	mm	2.0	-	-
Fertile pellet diameter	mm	7.07	14.36	-
Absorber pellet diameter	mm	-	-	17.0
Rod body outer diameter	mm	-	-	149.0
Rod body wall thickness	mm	-	-	2.0

Table III. Material volume fractions in the fuel zones of the core

Material	Volume fraction, %	
	Fissile SA	Radial breeder blanket SA
Fuel*	41.66	55.36
Pin cladding (accounting for spacer wire)	14.86	9.26
Hexcan	9.47	9.47
Sodium	34.01	25.92

(*) Fuel with smeared density

2.2.3. Core materials specification

There is a lack of detailed information available in open literature sources on the design of subassemblies and material content of the startup core. Most detailed information can be found in [5], [8] and [9]. Additional data on fuel composition can be found in [13]. There are curtain difference between number of fuel subassemblies and arrangement with respect to data, provided in [5]. The number of subassemblies in the inner and outer subcores and in radial breeder blanket is reduced as compared to data in [5] (see Table I), as it is noted in Fig. 2. Fuel composition data available in [5] has been taken as a basis for benchmark. The data on fuel composition in [8] is also evaluated for consistency and comparison. Nuclide number densities of materials used in the benchmark for as fabricated conditions are listed in Tables of Appendix A.

In [5], the total mass of Pu, mass of Pu-239 and mass of U-235 are provided for the fissile core volume, which are 5780 kg, 4054 kg and 142 kg respectively. Plutonium composition is not available in [5]. For the needs of benchmark the Pu composition has been constructed "from scratch" on the basis of the additional data, available in [13] on isotope vector of Pu, used in production of the fissile fuel. Pu isotope vectors for two contributions, from GGR and PWR reactors spent fuel, as provided in [13] are summarized in Table IV. These two contributions have been used to construct the Pu vector for the fissile fuel in the benchmark, assuming similar Pu-239 content in plutonium, as it is defined in [5], which is about 70%. The mixture of Pu from GGR with 70% and Pu from PWR with 30% has been considered further for the benchmark core. Additionally, Am-241 isotope was included in the Pu vector with content of 1.38%mass to account for realistic fuel conditions, as in accord to [8]. Uranium vector has been also evaluated on basis of data in [5]. Reconstruction of the depleted uranium content for the fissile core results in a uranium vector provided in Table V, which contents 0.5%mass of U-235 isotope. There is no corresponding data available for the fertile fuel. Depleted uranium with mass content of 0.25% has been taken.

There are certain differences with the fuel composition data in [9] with respect to Pu vector and depleted uranium vector in fissile fuel. In [9], the Pu-239 content is somewhat different, namely, about 67%mass and 70%mass in the inner and outer subcores respectively, and content of U-235 in the depleted uranium of fissile fuel is about 0.4%mass, while for the fertile fuel the same depleted uranium is used with U-235 content of 0.25%. The fuel enrichments, as in accord to definition [5] (see Table I), of the fissile fuel of the inner and outer subcores in [8] are equal to 16.3 and 19.4% respectively, what differs from the values given in [5]. With the use of this fuel specification the criticality level calculated by CEA for the hot nominal operating conditions equal to about 2400 pcm is somewhat higher than the evaluated value of about 2090 pcm, as in accord with [6] and [7].

The theoretical densities (TD) of plutonium and uranium oxides used in the benchmark are listed in Table VI. The porosity of both fissile and fertile fuel is equal to 95.5%, as given in [5]. The stoichiometry ratio of both oxides is set to 1.98. Applying the fuel specification constructed as described above with the fuel enrichments as given in Table I for the isothermal core conditions at 180°C, the core criticality level for the benchmark model also exceeds the experimentally observed value of 3710 pcm [6] (the value of 3950 pcm can be found in [2]). Thus it has been decided to reduce the fuel enrichments in the inner and outer subcores to values of 15.48% and 19.07% respectively, keeping the same ratio between two values of 0.812 as in [5] to profile the radial power release distribution. The composition of the 316Ti construction steel which is the only steel used in the model is given in Table VII. The physical densities of the 316Ti steel and boron carbide of the control rod absorber are given in Table VI. Sodium density in HET regions is calculated as follows [14]:

$$\rho_{Na}[g/cm^3] = (219.0 + 275.32 \cdot (1 - T/2503.7) + 511.58 \cdot (1 - T/2503.7)^{0.5}) \cdot 10^{-3},$$

where T is sodium temperature in K.

Table IV. Pu isotopic vectors used in the benchmark

Isotope	Content, %mass		
	Pu from GGR	**Pu from PWR**	**Pu mixture used in benchmark**
Pu-238	0.00	1.70	0.50
Pu-239	76.70	56.50	69.67
Pu-240	20.10	23.60	20.86
Pu-241	2.80	12.50	5.63
Pu-242	0.40	5.70	1.96
Am-241	-	-	1.38

Table V. Uranium isotopic vectors used in the benchmark

Isotope	Content, %mass	
	Fissile fuel	**Fertile fuel**
U-235	0.005	0.0025
U-238	0.995	0.9975

Table VI. Densities of the solid materials (at 20°C)

Material	UO_2	PuO_2	316Ti steel	B_4C
Density, g/cm^3	10.970*	11.460*	7.95	2.400*

(*)Theoretical density

Table VII. Composition of 316Ti construction steel used in the benchmark

Element	Cr	Ni	Mo	Mn	Si	C	Ti	P	Fe
Content, %mass	16.0	14.0	2.5	1.7	0.6	0.05	0.4	0.03	64.72

2.2.4. Approach on thermal expansion of core elements

Few assumptions have been used in order to obtain temperature expanded core geometry, as listed below:

- All steel elements of the core expand axially and radially with the linear expansion coefficient of the 316Ti steel, which is defined hereafter below. The steel density is corrected in accord to this expansion.
- Radial expansion of the diagrid which defines the subassembly pitch in the model is calculated with use of linear expansion coefficient of 304L steel, in accord to design of the core.
- For the calculation of fuel expansion the fuel pellet stack height is only modified in accord with linear expansion coefficient of MOX fuel, which is defined hereafter below. The radial dimensions of the fuel pellet have been kept as fabricated and the fuel density is modified correspondingly, to keep the fuel mass constant.
- Fuel pellet stack expansion is calculated individually from cladding expansion assuming conditions with no contact and mechanical interaction between fuel pellet and cladding.
- The homogenized compositions HOM in the model (see Fig. 3) are expanded with the 304L diagrid steel expansion coefficient in plane and with the 316Ti steel expansion coefficient axially, assuming material mass conservation. It is to notice that due lack of design the assumption may lead to not fully realistic variation of material masses in the volume (i.e. sodium).
- Boron carbide pellet stack is also expanded with corresponding linear expansion coefficient ensuring mass conservation.

In accord to these assumptions, fuel lower boundary is defined at unique level for both fissile and breeder subassemblies for any expanded configuration, while the upper boundary may vary, if different fissile and fertile temperatures are used.

For calculation of linear dimension change of the materials due to an increase of temperature from the reference temperature of 20°C (0°C for MOX) to the operational temperatures the equations for the mean linear expansion coefficients presented in Table VIII was used.

Table VIII. Linear expansion coefficients for the materials used in the benchmark

Material	**Ref.**	**Linear expansion coefficient, K^{-1}; temperature T in K**
MOX fuel	[15]	$9.828 \cdot 10^{-6} - 6.39 \cdot 10^{-9} \cdot T + 1.33 \cdot 10^{-12} \cdot T^2 - 1.757 \cdot 10^{-17} \cdot T^3$, $273K \leq T \leq 923K$ $1.1833 \cdot 10^{-5} - 5.013 \cdot 10^{-9} \cdot T + 3.756 \cdot 10^{-12} \cdot T^2 - 6.125 \cdot 10^{-17} \cdot T^3$, $923K \leq T \leq 3120K$
316Ti steel	[16]	$1.294 \cdot 10^{-5} + 9.354 \cdot 10^{-9} \cdot T - 3.314 \cdot 10^{-12} \cdot T^2$
304L steel	[16]	$1.216 \cdot 10^{-5} + 9.877 \cdot 10^{-9} \cdot T - 3.323 \cdot 10^{-12} \cdot T^2$
B_4C	-	$5.0 \cdot 10^{-6}$

2.3. Expected Results

2.3.1. Reference core configurations for core model validation

The following three core configurations have been selected for the modelling as reference for criticality prediction:

- Case1: "180°C". It is a first critical core configuration after all subassemblies of the first core were loaded. The core criticality is evaluated at level of 3710 pcm [6] with all control rods withdrawn at the top of fissile height. To model this configuration all the core elements dimensions and material densities are calculated as at 180°C and the isotope temperatures have been set to 453 K.

- Case 2: "HZP". This core state is defined as an isothermally heated-up core at 400°C and has been considered during startup tests, in particular, for evaluation of the isothermal reactivity coefficient k_{iso} for the range of core temperatures between 180°C and 400°C. The criticality level for this configuration has been evaluated on the basis of the given experimental value of k_{iso} [7] and set to 3079 pcm[†] with all control rods at the parking position (at the top of the fissile height). To model this configuration all the core elements dimensions and material densities are calculated as at 400°C and the isotope temperatures have been set to 673 K.

- Case 3: "HFP". The core at hot full power conditions has been considered with all fissile fuel at 1227°C and all fertile fuel at 627°C, while the rest of materials in the core are kept at 400°C. The criticality level for this configuration has been evaluated as follows. Assuming reactivity drop of about 1620 pcm with regard to 180°C, as can be assessed from [7], the criticality at HFP configuration is evaluated at level of 2090 pcm with all control rods withdrawn at the top of fissile height. To model this configuration all the core elements dimensions and material densities, except fuel pellet stack, are calculated as at 400°C and the isotope temperatures have been set to 673 K. The fissile fuel pellet stack height is calculated as at average temperature of 1227°C, while all fertile fuel in the axial and radial blankets is modelled at 627°C. Correspondingly, the fuel isotope temperatures are set to 1500 K and 900 K respectively for fissile and fertile fuels.

2.3.2. Static neutronics core performance and comparison with experimental data

As a first part of the benchmark, following core characteristics have been evaluated in current study:
- Core criticality at reference and benchmark configurations.
- CSD rods worth: As it can be found in [12], the total weight of all CSD rods is experimentally evaluated at level of 8630 pcm for the "180°C" core configuration.
- Reactivity coefficients: Isothermal coefficient, its expansion component and its component related to Doppler effect have been evaluated experimentally during startup tests for core transition from 400°C to 180°C [7]. These values are calculated in current study using expansion laws for the core described above.
- Reaction rates: Specific fission reaction rates have been measured during startup tests for evaluation of axial and radial neutron flux distribution in the core with help of fission foils with U-235, U-238 and Pu-239 [17]. The core and axial blanket reaction rate distributions were measured by irradiating several special subassemblies at 3 MW for 2 hours. In current study there is an attempt done to reproduce those measurements performed at T_1 core configuration [17], which considers all CSD

[†] evaluated as follows: K_{eff}("HZP") = K_{eff}("180°C") – (2.87 $pcm/°C \cdot 220°C$) = 3079 pcm

control rods uniformly inserted in the core keeping reactor at critical state. More particular, results of calculations will be compared to the following measurements results:

- Axial profile of the U-235 fission rate profile obtained in the SA of the inner subcore in 7th row located close to the boundary between inner and outer subcores (marked by a black circle in Fig. 2);
- Radial fission rate of U-238 at the fissile height slightly above the level of the critical control rod position (157.4 cm as in [17]);
- Radial fission rate of Pu-239 at about the middle of Upper Axial Blanket height (193.5 cm as in [17]).

2.3.3. Reactivity feedback effects and branch calculations

The reactivity coefficients suggested for evaluation in the benchmark are as follows:

– Doppler constant [pcm], calculated zone-wise;
– Sodium density coefficient [pcm/°C], calculated zone-wise;
– Axial fuel expansion [pcm/°C], calculated for inner subcore, outer subcore and radial blanket;
– Clad expansion coefficient [pcm/°C];
– Hexcan expansion coefficient [pcm/°C];
– Diagrid expansion coefficient [pcm/°C].

Their detailed definitions for modelling in the benchmark are to be formulated later on. In addition, some assumptions are necessary and will be formulated for definition of control rod drive lines (CRDL), strongback and vessel wall expansion coefficients (all in pcm/°C). These contributions depend on the control rod critical position and on models assumed for account for thermal inertia of structure and differential expansion of the vessel and its components. In current study these effects have not been evaluated, except the global core Doppler constant for different conditions.

3. CALCULATION RESULTS WITH SERPENT 2 MONTE CARLO CODE

The described model has been implemented as an input file for the Serpent 2 code, a 3D continuous-energy Monte Carlo particle transport code for reactor physics application, continuously being developed by the VTT Technical Research Centre of Finland since 2004 [18]. The JEFF311 library was used in the calculations presented below. A temperature-dependent model has been created applying the expansion laws as described above. Input preparation is facilitated by means of the TSP tool [19]. Calculations have been performed on CSCS Cray XC40 supercomputer with $7 \cdot 10^6$ source neutrons in one cycle and $4 \cdot 10^3$ active cycles, resulting in standard deviation of multiplication factor of about 1 pcm.

3.1. Criticality

Results of criticality calculations for different cases are listed in Table IX. An appropriate agreement with experimentally measured values can be stated for all reference configurations. Using the two calculations (cases 1 and 13) for “180°C” core configuration – with all CSD control rods withdrawn and located at the top of the fissile height and fully inserted till bottom of the fissile height – the CSD control rods total weight has been evaluated at level of 8661 pcm. This value is in agreement with experimentally observed value of 8630 pcm [12]. The HZP configuration with inserted CSD control rods by 40 cm (case 12) is considered as reference critical configuration for evaluation of fission reaction rates in the core.

Set of calculations presented in Table IX is intended for evaluation of Doppler constant and may serve as a basis for benchmark code-to-code comparisons. It includes cases linked to reference temperature libraries thus allowing to avoiding inaccuracies due to Doppler effect evaluation for intermediate temperatures. Three kinds of Doppler constant (Table X) have been evaluated based on the data in

Table IX on criticality for different cases. First two lines of the Table X are the Doppler constants related to isothermal core heat-up and thus characterise Doppler effect on all isotopes in the core, including contribution of the construction steel isotopes. Next, the fuel Doppler constant has been evaluated, assuming all fuel isotopes temperature rise up to 600 K. One can conclude that calculated Doppler effect on construction steel isotopes (mainly Fe) is 8.4% of the total effect and results in increases of absolute value of Doppler constant by 116 pcm. In current calculations this effect contributes to the Doppler component of isothermal expansion reactivity effect described in next section. Last value presented in Table X is obtained for the identical fuel heat-up assuming critical core configuration with inserted by 40 cm control rods. Insertion of control rods decreases the Doppler constant by 48 pcm or 3.5%. This effect has to be considered comparing the experimentally observed and calculated values of isothermal expansion coefficient.

Table IX. Criticality of the core at different configuration

Case ID	CSD insertion* [cm]	Temperature for XS/geometry [K]			Calculated		Measured reactivity [pcm]	C – E [pcm]
		Fissile	Fertile	Other	k-eff [-]	Reactivity [pcm]		
1	0	453/453	453/453	453/453	1.03668	3538	3710	-170
2	0	673/673	673/673	673/673	1.02886	2805	3079	-274
3	0	1500/1500	900/900	673/673	1.01903	1867	2090	-223
4	0	300/293	300/293	300/293	1.04362	4180	-	-
5	0	300/453	300/453	300/453	1.04246	4073	-	-
6	0	300/673	300/673	300/673	1.04080	3920	-	-
7	0	600/673	600/673	600/673	1.03053	2963	-	-
8	0	900/673	900/673	900/673	1.02483	2423	-	-
9	0	600/673	600/673	300/673	1.03139	3043	-	-
10	40	300/673	300/673	300/673	1.00824	817	-	-
11	40	600/673	600/673	600/673	0.99893	-107	-	-
12	40	673/673	673/673	673/673	0.99742	-258	-	-
13	100	453/453	453/453	453/453	0.95127	-5131	-	-

(*) From the top of fissile height

Table X. Doppler constant for different conditions

Calculation case	Value [pcm]
Case 6 – Case 7	-1381 ± 2
Case 6 – Case 8	-1363 ± 2
Case 6 – Case 9	-1265 ± 2
Case 10 – Case 11	-1334 ± 2

3.2. Isothermal Expansion Coefficient

For evaluation of the isothermal expansion coefficient two configurations have been considered: “180°C” and “HZP” (cases 1 and 2 in Table IX). In accord to the definition given above, both configurations assume CSD control rods withdrawn up to the top of the fissile height. It means there is no control rods related contribution in the calculated effect. Assuming isothermal heat-up and expansion of all reactor structures, like vessel, diagrid, strongback, core, control rod drive lines, the influence of control rod and core mutual displacement is considered as very limited. Transition of the core from “180C” to “HZP” leads to drop of the reactivity by –735 pcm. Corresponding value of isothermal temperature coefficient k_{iso} is equal to 3.34 pcm/°C (Table XI).

The expansion component has been evaluated on the basis of two calculations with different geometry applying identical cross section library (cases 5 and 6 in Table IX). With no account for effect of control

rods, there is an appropriate agreement stated with experimentally evaluated value. Doppler component is the main contribution of the isothermal expansion effect and evaluated as at first line of Table X. The isothermal coefficient calculated using the two component contributions is equal to 3.18 pcm/°C. This difference is resulted from the calculation of Doppler broadening of resonances by the Serpent 2 code for exact temperatures used in two reference core states (453 K and 673 K).

Table XI. Isothermal expansion coefficient and its components

Parameter	Benchmark*	Calculation [7]	Experiment [7]
Isothermal temperature coefficient (400–180°C) [pcm/°C]	3.34 (3.18**)	2.63 ± 0.53	2.87 ± 0.14
Expansion component k [pcm/°C]	0.70	0.67 ± 0.23	0.74 ± 0.15
Doppler component K_D [pcm]	1381	1086 ± 217	1180 ± 118

(*) Calculations do not consider inserted CRs and differential effect of CR movement due temperature expansion of the vessel and its inner structures

(**) Calculated value as sum of two individual components

Considering control rods at critical position and reduced Doppler constant, the corresponding absolute value of the Doppler component is reduced by 19 pcm. It results in a reduction of the isothermal temperature coefficient by about 0.1 pcm/°C and gives value of 3.10 pcm/°C, what is closer to the experimentally evaluated value. Introduction of the control rods effect may also influence the expansion component. Withdrawal of CRs by 25 pcm (about 2 mm) as result of differential core vessel and its inner structures expansion would lead to correction of the expansion component by -0.12 pcm, resulting in a value of 0.58 pcm/°C. Together with corresponding Doppler constant reduction due to CR critical position it would result in isothermal temperature coefficient equal to -2.98 pcm/°C what is good within experimentally observed uncertainty.

Few additional remarks are of importance for analysis performed above. Firstly it should be noted that particular uncertainty is introduced in the calculated isothermal coefficient by poor assumption on modelling of the expansion of the diluent and radial reflector zones and compositions. It is hardly possible to predict, how knowing of the detailed geometry would influence the expansion component. This effect is considered as almost negligible. Second remark is related to uncertainty of the modelled fuel with respect to realistic situation. Regarding Doppler effect dependence on fuel content, in particular, on fuel enrichment and quality of Pu vector, for higher Pu mass content in the fuel and different Pu vector the evaluations of Doppler constant have been performed, which are not reported here. The Doppler constant absolute value may deteriorate by up to 100 pcm, what would also lead to decrease of the isothermal coefficient by about 0.3 pcm/°C. Last remark is general and is related to nuclear data library choice. Analysis revealed that application of ENDF-B/VII library results in a lower by about 500 pcm multiplication factor for reference core states. Application of this library would require increase of the Pu enrichment in the core to reach the reference criticality levels.

3.3. Reaction Rates

For calculation of the reaction rates as proposed by the benchmark the number of the detectors has been placed into the Serpent 2 model. Fig. 7a presents the axial profile of the U-235 fission rate calculated for HZP critical core configuration as compared to the data provided in [17]. The close to critical position of the CSD control rods inserted by 40 cm is shown in Fig. 7a. Both profiles have been normalized to make maximum value equal to 1. There is an appropriate agreement between the fission rate profiles in the modelled core and experimental data for the whole fuel height, which includes lower axial blanket, fissile height and upper axial blanket. Fig. 7b demonstrates the radial profile of the U-238 fission rate at fissile height for HZP core configuration with CRs inserted by 40 cm. The detector axial position in the model is chosen in accord to the axial position of the experimental foils, which was about 20 cm below top of the

fissile height. Both profiles have been normalized to make the maximum value equal to 1. The experimental points include arbitrary chosen 3% error bars, while for the calculated values the statistical error is relatively small (below 0.2%). There is also appropriate agreement between the radial fission rate profiles obtained at the fissile height in the modelled core and in the experiment. Fig. 7c shows the radial profile of the Pu-239 fission rate in the upper axial blanket. The detector axial position in the model is chosen in accord to the axial position of the experimental foils, which was about 15 cm above the top of fissile height. Both profiles have been normalized to the maximum value equal to 1. The experimental points include 3% error bars, while for the calculated values the statistical error is relatively small (below 0.4%). There is also appropriate agreement between the radial fission rate profiles obtained at the fertile fuel in the modelled core and in experiment.

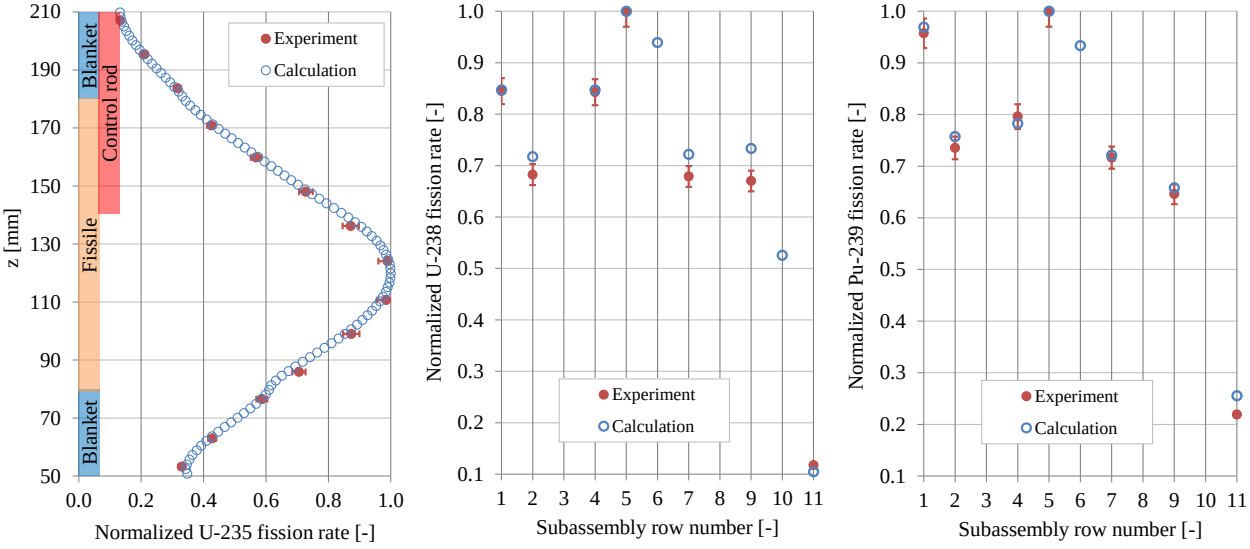

a) b) c)

Figure 7. Comparison of calculated results with measured data normalized to 1 for Case 12 (HZP core configuration with CRs inserted by 40 cm): (a) axial fission rate profile of U-235; (b) radial fission rate profile of U-238 in fissile region; (c) radial profile of Pu-239 fission rate in upper blanket

4. CONCLUSIONS

The paper summarizes the definition and preliminary results of a new benchmark on Superphénix reactor startup core. The detailed definition of the heterogeneous core model is given as constructed on the basis of available open literature sources. The preliminary evaluation of core neutronics performance is presented, including prediction of the core criticality at different configurations, some reactivity feedback characteristics of the core and spatial distributions of the reaction rates for evaluation of the neutron flux shape in the core. Some values have been compared with experimentally observed ones.

It has been demonstrated, that chosen assumptions and design data for establishing of the benchmark allow representing the experimentally observed characteristics of the startup core. Observed differences with experimental values and the possible reasons are also discussed. The values calculated in this phase of benchmark can be used for code-to-code and library comparison.

The model is intended for further benchmark analysis, in particular, for calculation of reactivity feedback contributions and reactivity coefficient set for the transient analysis.

ACKNOWLEDGMENTS

The work has been prepared within EU Project ESFR-SMART which has received funding from the EURATOM Research and Training Programme 2014-2018 under the Grant Agreement No. 754501.

Calculations have been performed with use of Cray XC40 supercomputer resources supported by a grant from the Swiss National Supercomputing Centre (CSCS) under Project s771 "Generation-IV European Sodium Fast Reactor: Computation of the Core Parameters Using a High-Fidelity Monte Carlo Code".

REFERENCES

1. Generation IV International Forum Web-page http://www.gen-4.org.
2. J. Guidez, G. Prêle, *Superphenix: Technical and Scientific Achievements*, Atlantis Press and the author(s) 2017, ISBN 978-94-6239-246-5.
3. K. Mikityuk, E. Girardi, J. Krepel, E. Bubelis, E. Fridman, A. Rineiski, N. Girault, F. Payot, L. Buligins, G. Gerbeth, N. Chauvin, C. Latge, J.-C. Garnier, "ESFR-SMART: new Horizon-2020 project on SFR safety", IAEA-CN-245-450, *Proceedings of International Conference on Fast Reactors and Related Fuel Cycles (FR'17)*, Yekaterinburg, Russia, June 26-29, 2017.
4. K. Mikityuk and M. Schikorr, "New Transient Analysis of the Superphénix start-up Tests", *Proceedings of International Conference on Fast Reactors and Related Fuel Cycles: Safe Technologies and Sustainable Scenarios (FR'13)*, Paris, France, March 4-7, 2013.
5. "Fast Reactor Database", IAEA-TECDOC-866, IAEA, Vienna, Austria, February 1996.
6. G. Flamenbaum, R. de Wouters, A. Le Bourhis, T. Newton and G. Vambenepe, "Superphenix Core-Loading Strategy Using the Checkerboard Pattern," *Nuclear Science and Engineering*, **106**, pp. 11-17 (1990).
7. M. Vanier, P. Bergeonneau, J. C. Gauthier, M. Jacob, J. De Antoni, E. Gesi, P. Peerani and J. P. Adam, "Superphenix Reactivity Feedback And Coefficients", *Nuclear Science and Engineering*, **106**, pp. 30-36 (1990).
8. "Superphenix Benchmark used for Comparison of PNC and CEA Calculation Methods, and of JENDL-3.2 and CARNAVAL IV Nuclear Data", O-Arai Engineering Center, Power Reactor and Nuclear Fuel Development Corporation, 1998.
9. J. Gourdon and B. Mesnage, "An Overview of Superphenix Commissioning Tests," *Nuclear Science and Engineering*, **106**, pp. 1-10 (1990).
10. J. P. Girard, H. Recroix, M. J. Beesley, G. Weinkoetz, L. Krebs, R. S. Overton and G. Hughes, "Detection of Coolant Temperature Noise in SPX1 Using Intrinsic High Frequency Thermocouples", *Progress in Nuclear Energy,* **21**, pp. 377-392 (1988).
11. J. D. B. Lambert and R. Strain, *Oxide Fuels,* p. 126, Materials Science and Technology (2006).
12. J. C. Gauthier, J. C. Cabrillat, G. Palmiotti, M. Salvatores, M. Giese, M. Carta and J. P. West, "Measurement and Predictions of Control Rod Worth", *Nuclear Science and Engineering*, **106**, pp. 18-29 (1990).
13. D. Doutriaux, G. Kyriazidis, G. Rimpault, S. Pilate, V. Rouyer and B. Blan, "Data and Methods Used to Assess the Subcriticality of the Storage of Unirradiated Superphenix Subassemblies, ICNC99, 1999.
14. J. K. Fink and L. Leibowitz, "Thermodynamical and Transport Properties of Sodium Liquid and Vapor", Argonne National Laboratory, Division of Reactor Engineering, 1995.
15. S. G. Popov, J. J. Carbajo, V. K. Ivanov and G. L. Yoder, "Thermophysical Properties of MOX and UO_2 Fuels Including the Effects of Irradiation", Oakridge National Laboratory, 2000.
16. P. D. Desai and C. Y. Ho, "Thermal Linear Expansion of Nine Selected AISI Stainless Steels", Center for Information and Numerical Data Analysis and Synthesis, Purdue University, 1978.
17. J. C. Cabrillat, M. Martini, "Power and Neutron Flux Distributions in the Core and Shielding", *Nuclear Science and Engineering*, **106**, pp. 37-46 (1990).
18. J. Leppänen, M. Pusa, T. Viitanen, V. Valtavirta, T. Kaltiaisenaho, "The Serpent Monte Carlo code: Status, development and applications in 2013", *Annals of Nuclear Energy*, **82**, pp. 142-150 (2015).
19. A. Travleev, "TSP: Python Package to Facilitate Preparation of Input Files", Internal report INR 31/13 – NUKLEAR 3462, KIT, Karlsruhe, Germany, November 2013.

APPENDIX A.

Table A.I. As-fabricated isotope number densities of the fuel, $\times 10^{24}$ 1/cm^3

Isotope	Inner subcore fuel	Outer subcore fuel	Fertile fuel
U-235	1.01274E-04	9.71287E-05	5.92251E-05
U-238	1.98991E-02	1.90845E-02	2.33323E-02
Pu-238	1.78335E-05	2.21382E-05	-
Pu-239	2.45976E-03	3.05349E-03	-
Pu-240	7.33391E-04	9.10417E-04	-
Pu-241	1.97174E-04	2.44768E-04	-
Pu-242	6.84331E-05	8.49515E-05	-
Am-241	4.82584E-05	5.99070E-05	-
O	4.65798E-02	4.66433E-02	4.63152E-02

Table A.II. As-fabricated isotope number densities of non-fuel core materials, $\times 10^{24}$ 1/cm^3

Isotope	316Ti steel	90% boron carbide	Diluent	Radial shielding
C-nat	1.99483E-04	2.46696E-02	-	-
Si-28	9.46910E-04	-	6.22000E-04	4.23000E-04
Si-29	4.64444E-05	-	3.15000E-05	2.14000E-05
Si-30	2.96324E-05	-	2.09000E-05	1.42000E-05
P-31	4.63709E-05	-	-	-
Ti-46	3.43812E-05	-	2.30000E-05	1.57000E-05
Ti-47	3.03458E-05	-	2.10000E-05	1.43000E-05
Ti-48	2.94438E-04	-	2.12000E-04	1.44000E-04
Ti-49	2.11661E-05	-	1.58000E-05	1.08000E-05
Ti-50	1.98618E-05	-	1.55000E-05	1.06000E-05
Cr-50	6.66387E-04	-	2.19418E-04	3.32910E-04
Cr-52	1.23572E-02	-	4.23704E-03	6.41983E-03
Cr-53	1.37473E-03	-	4.80447E-04	7.27957E-04
Cr-54	3.35867E-04	-	1.19593E-04	1.81204E-04
Mn-55	1.48147E-03	-	9.40570E-04	6.39840E-04
Fe-54	3.35763E-03	-	1.01918E-03	1.54425E-03
Fe-56	5.08275E-02	-	1.61170E-02	2.44205E-02
Fe-57	1.15320E-03	-	3.86584E-04	5.85750E-04
Fe-58	1.50826E-04	-	4.92016E-05	7.45500E-05
Ni-58	7.87595E-03	-	2.51082E-03	3.80428E-03
Ni-60	2.93277E-03	-	9.64157E-04	1.46539E-03
Ni-61	1.25393E-04	-	4.20455E-06	6.37055E-06
Ni-62	3.93381E-04	-	1.34029E-04	2.03075E-04
Ni-64	9.70357E-05	-	3.41527E-05	5.17467E-05
Mo-92	1.89224E-04	-	6.57917E-05	9.96832E-05
Mo-94	1.16625E-04	-	4.10090E-05	6.21341E-05
Mo-95	1.99765E-04	-	7.05797E-05	1.06938E-04
Mo-96	2.08043E-04	-	7.39491E-05	1.12043E-04
Mo-97	1.18571E-04	-	4.23390E-05	6.41493E-05
Mo-98	2.98169E-04	-	1.06978E-04	1.62086E-04
Mo-100	1.17644E-04	-	4.26936E-05	6.46866E-05
Cu-63	-	-	1.31000E-04	8.93000E-05
Cu-65	-	-	5.85000E-05	3.98000E-05
B-10	-	8.88105E-02	-	-
B-11	-	9.86783E-03	-	-
Na-23	-	-	5.76350E-03	1.09310E-02